Hybrid systems combining liposomes and entangled hyaluronic acid chains: Influence of liposome surface and drug encapsulation on the microstructure

Céline Jaudoin, Isabelle Grillo, Fabrice Cousin, Maria Gehrke, Malika Ouldali, Ana-Andreea Arteni, Luc Picton, Christophe Rihouey, Fanny Simelière, Amélie Bochot, et al.

Hybrid systems combining liposomes and entangled hyaluronic acid chains: influence of liposome surface and drug encapsulation on the microstructure

Céline JAUDOIN [a], Isabelle GRILLO [#b], Fabrice COUSIN [#c], Maria GEHRKE [a], Malika OULDALI [d], Ana-Andreea ARTENI [d], Luc PICTON [e], Christophe RIHOUEY [e], Fanny SIMELIERE [a], Amélie BOCHOT [§a], Florence AGNELY [§a*]

[a] Université Paris-Saclay, CNRS, Institut Galien Paris-Saclay, 5 rue J-B Clément, 92296 Châtenay-Malabry, France. celine.jaudoin@universite-paris-saclay.fr, m.s.gehrke@hotmail.de, fanny.simeliere@universite-paris-saclay.fr, amelie.bochot@universite-paris-saclay.fr, florence.agnely@universite-paris-saclay.fr

[b] Institut Laue-Langevin, 71 avenue des Martyrs, 38042 Grenoble, France.

[c] Laboratoire Léon Brillouin, Université Paris-Saclay, UMR12 CEA-CNRS, 91191 Gif-sur-Yvette, France. fabrice.cousin@cea.fr

[d] Université Paris-Saclay, CEA, CNRS, Institute for Integrative Biology of the Cell (I2BC), 91198, Gif-sur-Yvette, France. malika.ouldali@i2bc.paris-saclay.fr, ana-andreea.arteni@i2bc.paris-saclay.fr

[e] Laboratoire Polymères, Biopolymères, Surfaces (PBS), UMR CNRS 6270, Normandie University, UNIROUEN, boulevard Maurice de Broglie, 76821 Mont-Saint-Aignan, France.

luc.picton@univ-rouen.fr, christophe.rihouey@univ-rouen.fr

[#]Same contribution. [§]Same contribution

*Corresponding author, e-mail: florence.agnely@universite-paris-saclay.fr, telephone: +33 1 46 83 56 26

We dedicate this publication to the memory of Dr. Isabelle Grillo, who left us in august 2019. Isabelle was a kind, pedagogue, and recognized scientist. With her enthusiasm, she took us into the neutronic world, and we will try to acknowledge her work in this article.

Abbreviations [1]

[1] **Abbreviations**: C*, overlap concentration; Ce, entanglement concentration; Chol, cholesterol; cryo-EM, electron cryomicroscopy; DexP, dexamethasone phosphate; DexP-LipPEG, dexamethasone phosphate-loaded PEGylated liposomes; DLS, dynamic light scattering; DSPE, 1,2-distearoyl-sn-glycero-3-phosphoetanolamine; EPC, egg phosphatidylcholine; FRAP, fluorescence recovery after photobleaching; HA, hyaluronic acid; HEPES, 4-(2-hydroxyethyl)piperazine-1-ethanesulfonic acid; Lip, neutral liposomes; Lip^-, anionic liposomes; Lip^+, cationic liposomes; LipPEG, PEGylated liposomes; PdI, polydispersity index; PEG, poly(ethylene glycol); PG, egg L-a-phosphatidylglycerol; SA, stearylamine; SANS, small angle neutron scattering; SEC, size-exclusion chromatography.

Abstract

Mixtures of hyaluronic acid (HA) with liposomes lead to hybrid colloid–polymer systems with a great interest in drug delivery. However, little is known about their microstructure. Small angle neutron scattering (SANS) is a valuable tool to characterize these systems in the semi-dilute entangled regime (1.5% HA) at high liposome concentration (80 mM lipids). The objective was to elucidate the influence of liposome surface (neutral, cationic, anionic or anionic PEGylated), drug encapsulation and HA concentration in a buffer mimicking biological fluids (37 °C). First, liposomes were characterized by SANS, electron cryomicroscopy, and dynamic light scattering and HA by SANS, size exclusion chromatography, and rheology. Secondly, HA-liposome mixtures were studied by SANS. In HA, liposomes kept their integrity. Anionic and PEGylated liposomes were in close contact within dense clusters with an amorphous organization. The center-to-center distance between liposomes corresponded to twice their diameter. A depletion mechanism could explain these findings. Encapsulation of a corticoid did not modify this organization. Cationic liposomes formed less dense aggregates and were better dispersed due to their complexation with HA. Liposome surface governed the interactions and microstructure of these hybrid systems.

Keywords: cryo-electron microscopy, depletion, drug encapsulation, hyaluronic acid, hybrid systems, liposomes, microstructure, semi-dilute entangled regime, small angle neutron scattering, surface.

Graphical abstract

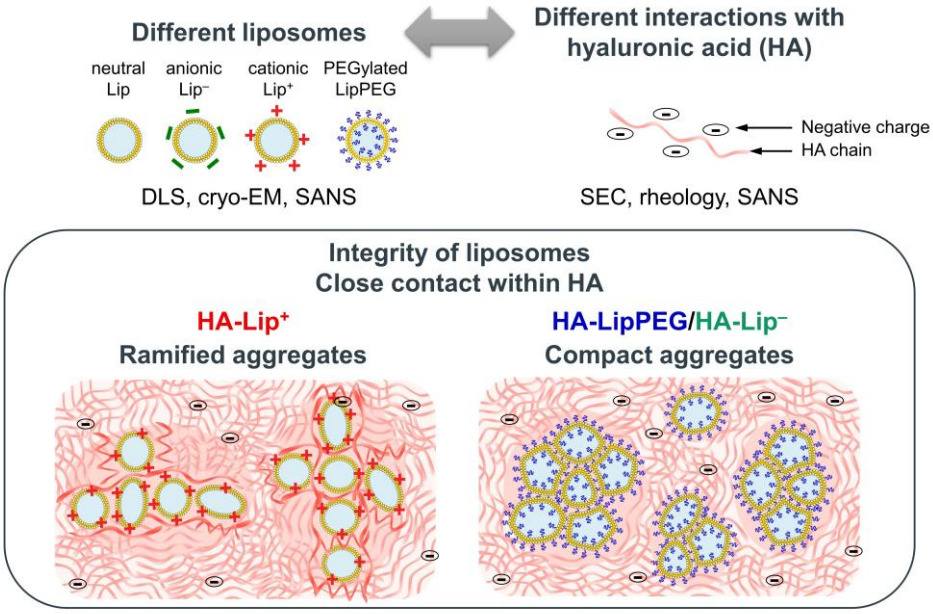

1. Introduction

In drug delivery, nanocarriers provide numerous advantages over conventional forms. Indeed, they can sustain drug release, target specific organs, increase therapeutic index, and protect poorly-stable molecules. Among the nanomedicines on the market, liposomes are predominant due to their excellent safety profile and versatility [1]. These colloids consist of lipid bilayers surrounding one or several aqueous compartments, enabling the encapsulation of lipophilic and hydrophilic molecules respectively. Their size (50 nm to 5 µm) and surface are easily tunable. Researchers incorporate liposomes in polymer solutions or hydrogels to obtain locally injectable drug delivery systems [2,3]. Indeed, for some targeted tissues that are hardly accessible from the bloodstream, local therapies allow a higher dose and residence time for drugs.

Hyaluronic acid (HA) is a linear polyanionic polymer composed of N-acetyl-glucosamine and glucuronic acid units [4]. It is naturally present in the human body, highly biocompatible, and biodegradable. At high molar weights (> 500 kDa), this polymer possesses healing and mucoadhesive properties that are much valued in the medical field [5]. Furthermore, concentrated solutions of HA are easily injectable through fine needles thanks to their shear-thinning behavior. Such solutions are also very viscous, which increases the residence time of the system locally.

The mixture of HA with liposomes leads to hybrid colloid–polymer systems. They exhibit interesting properties and potential applications in drug delivery, particularly in otology [6] and ophthalmology [7]. Structural characteristics of smaller nanocarriers such as pluronic micelles (~20 nm with a narrow size distribution) combined with HA were already investigated by small-angle neutron scattering (SANS) [8]. However, little is known about hybrid systems involving liposomes, although SANS could provide crucial information on their microstructure.

From a fundamental perspective, colloid–polymer systems are organized into two classes: the "colloid limit" (large colloid-small polymer) and the "protein or nanoparticle limit" (small colloid-large polymer) [9,10]. The protein limit theory ($R_G/R_{colloid} > 1$, with R_G the polymer gyration radius and $R_{colloid}$ the colloid radius) is less established than its counterpart, the colloid limit ($R_G/R_{colloid} < 1$). In the colloid limit, a polymer depletion mechanism induces colloid aggregation. As the polymer cannot penetrate the colloidal particles, the entropy of the polymer is reduced. The polymer is excluded from a layer corresponding to R_G around the colloidal particles [11]. Polymer chains are also excluded when the polymer-depleted layers of two

adjacent colloids overlap. Due to this polymer depletion, an osmotic imbalance takes place, leading to particles aggregation. This phenomenon increases the available volume for polymer chains, increasing the depletion effect [10,12] and resulting in segregative phase separation.

For the protein limit ($R_G/R_{colloid} > 1$), experimental models are still lacking. Phase separation is also observed, but the polymer can also wrap around the smaller particles [13]. Many colloidal interactions are also implicated in addition to polymer-polymer interactions and polymer conformation [14]. The first scaling laws and models were developed by Sear [15–17] with the following hypothesis: (i) the polymer is in good solvent conditions and does not adsorb on particles, (ii) all interactions are considered as excluded volume ones. For non-adsorbing polymers, this segregation into colloid-rich and colloid-poor phases might result from the depletion effect that relies on excluded volume interactions [10,12]. This mechanism was often investigated for nonionic non-adsorbing polymers in the dilute regime. Polyelectrolytes in semi-dilute polymer regime have been rarely considered in the literature, although they have many applications in the pharmaceutical field.

This work investigates by SANS a pharmaceutical colloid–polymer system with more dispersity and complexity than model systems classically studied by this technique. Our hybrid system is composed of HA (high molecular weight) and liposomes (high lipid concentration), which maximizes the amount of drug administered [6]. This HA-liposome system has already demonstrated its ability to deliver drugs of different nature (peptides [7], antioxidants [18], and corticoids [6]) in animals. This study aims to evaluate the impact of the polymer on the integrity and organization of liposomes and the potential interference of an encapsulated hydrophilic drug in this organization.

The influence of liposome surface properties (neutral, cationic, anionic, or anionic and covered with poly(ethylene glycol) (PEG)), HA concentration, and the encapsulation of a corticoid (dexamethasone phosphate, DexP) on the microstructure of the HA-liposome system was evaluated in a saline buffer mimicking biological fluids (37°C, high salt limit, pH 7.4). Firstly, primary constituents of this hybrid system were characterized separately: liposomes by SANS, electron cryomicroscopy (cryo-EM), and dynamic light scattering (DLS); HA by SANS, size exclusion chromatography, and rheology. Secondly, HA-liposome mixtures were studied by SANS.

2. Materials and methods

2.1. Material

Sodium hyaluronate (HA) with a high molecular weight was provided by Acros Organics (M.W. supplier of $1.6.10^6$ g/mol, batch A0375841, purity 95% Geel, Belgium). 1,2-distearoyl-sn-glycero-3-phosphoethanolamine-N-[methoxy-poly(ethyleneglycol)-2000] (DSPE-PEG_{2000}) was obtained from Lipoids GmbH (Ludwigshafen, Germany). Egg phosphatidylcholine (EPC, purity 96%) was provided by Lipoid GmbH (Ludwigshafen, Germany). Dexamethasone sodium phosphate (purity 98%) was purchased from Fagron (Amsterdam, The Netherlands). Cholesterol (Chol), D_2O (99.9 atom % D), egg L-α-phosphatidylglycerol (PG), sodium chloride, stearylamine (SA), 4-(2-hydroxyethyl)piperazine-1-ethanesulfonic acid (HEPES), phosphoric acid, trichloroacetic acid, were obtained from Sigma-Aldrich Co. (St. Louis, USA). MilliQ water was used, with a resistivity of around 20 MΩ.cm (Millipore, Molsheim, France). All other chemicals were of analytical grade. The physical parameters of the different components of the formulations are detailed in Table 1.

Table 1. Physical parameters of the different chemicals used: chemical formula, ratio (if chemical mix), molecular weight M_w, density, neutron scattering length density ρ.

	Formula	Molar ratio	M_w (g/mol)	Density (g/cm^3)	ρ (neutron) (cm^{-2})
EPC	$C_{40}H_{80}NO_8P$ $C_{44}H_{84}NO_8P$	1:1	734 786	0.97*	0.22 10^{10}
Chol	$C_{27}H_{46}O$	–	387	1.07#	0.26 10^{10}
SA	$C_{18}H_{39}N$	–	270	0.86#	–0.33 10^{10}
PG	$C_{38}H_{74}O_{10}PNa$ $C_{42}H_{78}O_{10}PNa$	1:1	745 797	1.00‡	0.38 10^{10}
DSPE	$C_{41}H_{82}O_8P$	–	748	1.00‡	0.25 10^{10}
PEG (repeat unit)	C_2H_4O	–	44	1.01‡	0.55 10^{10}
Dexamethasone phosphate	$C_{22}H_{28}FNa_2O_8P$	–	516	1.32‡	1.63 10^{10}
HA (repeat unit)	$C_{28}H_{43}N_2O_{23}Na$	–	401	1.70⊥	2.31 10^{10}
Solvent	D_2O:HEPES:NaCl	99.2:0.2:0.6	20:238:58	1.10	6.33 10^{10}

Density values were taken in ⊥Grillo et al., 2020; #Haynes, 2016; *Rowe et al., 2009 or ‡approximated. Chol: cholesterol, DSPE: 1,2-distearoyl-sn-glycero-3-phosphoetanolamine, EPC: egg phosphatidylcholine, HA: hyaluronic acid, HEPES: 4-(2-hydroxyethyl)piperazine-1-ethanesulfonic acid, PEG: poly(ethylene glycol), PG: egg L-α-phosphatidylglycerol, SA: stearylamine.

2.2. Preparation of liposomes

Liposome suspensions with different surfaces (neutral: Lip; positively charged: Lip^+; negatively charged: Lip^-; PEGylated: LipPEG) were prepared by the thin-film hydration method (Bangham et al., 1965). Lipids (Table 2) were dissolved in chloroform, sampled with Hamilton syringes (Bonaduz, Switzerland) in appropriate amounts to reach a theoretical lipid concentration of 90 mM. They were mixed in an amber glass balloon, and chloroform was evaporated on a rotary evaporator BÜCHI R-124 at 100 mBar. The lipid film was hydrated with D_2O buffer (HEPES/NaCl 10/115 mM, pH 7.4) under vortex for 10 min. Extrusion through 0.2, 0.1, and 0.05 μm polycarbonate filters (LIPEX Extruder, Evonik Nutrition & Care GmbH, Vancouver, Canada) was used to reduce the size of liposomes and reach the targeted hydrodynamic diameter of 75 nm. Lip and Lip^+ suspensions were also sonicated for a few cycles of 15 min (pulse of 30 ms every 2 seconds) using a Branson 450 digital sonifier (Branson Ultrasonics Corporation, Danbury, USA).

Dexamethasone phosphate-loaded PEGylated liposomes (DexP-LipPEG) were also prepared, as previously described by El Kechai et al. (2016). Briefly, the lipid film was hydrated with dexamethasone phosphate solution at 100 mg/mL in D_2O. After extrusion on 0.2, 0.01, and 0.05 μm polycarbonate filters, the non-encapsulated fraction of dexamethasone phosphate was eliminated by dialysis with repeated medium changes for 48 h at 4 °C. A Gebaflex® dialysis bag with a molecular weight cut-off between 12 and 14 kDa (Interchim, Montluçon, France) was bathed in D_2O buffer (HEPES/NaCl 10/115 mM, pH 7.4). All samples were protected from light.

2.3. Liposome characterization

2.3.1. Size and zeta (ζ) potential determination

The liposomes' size and ζ potential were determined in triplicate at 25 °C using a Zetasizer Nano ZS (Malvern, Worcestershire, UK), after dilution of the liposomal suspensions to 2 mM of lipids with milliQ water. Each measurement was the average of at least 12 runs. The hydrodynamic diameter (D_h) was measured by dynamic light scattering (DLS) at the backscattering angle 173°, with refractive indexes of 1.45 and 1.33 respectively for dispersed material and solvent. The deviation of the mean was estimated through the polydispersity index (PdI) width (PdI width = z-average $\times \sqrt{PdI}$). This calculation was more relevant than the standard deviation of 3 different measures and allowed a better understanding of the distribution

of size in the suspension. PdI was obtained from the slope of the correlation function. The ζ potential was assessed at a count rate > 100 kcps and conductivity of around 0.3 $mS.cm^{-1}$. Liposomes were placed under an electric field, and their mobility was measured, related to the ζ potential using the Smoluchoswki equation [21].

2.3.2. Lipid quantification

EPC concentration was quantified by an enzymatic phospholipid assay (Biolabo SA, Maizy, France) after extrusion, sonication, or dialysis. Liposome suspensions were diluted to perform measurements in the validity range of the assay (0.22-10.75 mM). 10 µL of sample were incubated with 1 mL-enzyme reagent for 10 min in a water-bath at 37 °C (n = 2). Absorbance was measured at 500 nm (UV–Vis spectrometer Lambda 25, Perkin-Elmer, Waltham, USA). Assuming that the lipid ratios did not change during the different steps of liposome preparation, the total amount of lipids was calculated from EPC concentration (Eq. 1):

$$[Lipids] = \frac{A_{measured}}{A_0} \times \frac{Y[Lipids]_0}{M_{EPC} f_{EPC}} \times 10^3 \qquad \text{Eq. 1}$$

with A_0 and $[Lipids]_0$ respectively the absorbance and the lipid concentration (mM) of the standard solution, M_{EPC} and f_{EPC} respectively the molar mass (g/mol) and the molar fraction of EPC (mol/mol) in the EPC formulation, and Y the dilution factor of the liposomes. Suspensions were adjusted to 80 mM of lipids.

2.3.3. Cryogenic electron microscopy (cryo-EM)

The cryo-EM grids were prepared using a Vitrobot Mark IV (ThermoFisher) at 20 °C and 100% humidity. 3 µL of sample were applied onto freshly glow-discharged Quantifoil grids (R2/2), 200 mesh grids. The grids were blotted for 7 s with blot force 2, then plunge-frozen in liquid-nitrogen-cooled ethane. Cryo-EM images were observed in a Tecnai G2 FEG electron microscope (ThermoFischer) operating at 200 kV and equipped with a DDC K2 Summit direct-detection camera (Gatan Inc.). Images were recorded at 15 000× magnification, with a pixel size of 2.5 Å at the specimen level and 20 $e^-/Å^2$. The mean horizontal diameter was determined for each liposome suspension on cryo-EM pictures using ImageJ 1.52a software (Wayne Rasband, USA). On several images, the horizontal diameter (D_{EM}), shell thickness (lipid bilayer) ($t_{s\,(EM)}$), and the mean number of shells per vesicle (N_s) were systematically measured,

with more than 300 compiled measures for each type of liposome. The PdI was estimated from data dispersity as follows:

$$PdI = \left(\frac{\text{standard deviation}}{D_{EM}} \right)^2 \qquad \text{Eq. 2}$$

2.4. Multi-detection coupled on-line size-exclusion chromatography

HA solutions were prepared or diluted at 0.1 $g.L^{-1}$ in the eluent and filtered on a 0.45 μm filter (regenerated cellulose). Number-average molar mass (M_n), weight-average molar mass (M_w), and dispersity (Đ) were determined by size exclusion chromatography coupled with multiangle light scattering detector, a viscosity detector, and a refractive index detector. The whole line was equipped with an online degasser, a pump (LC10Ai, Shimadzu, Japan) with a flow rate of 0.5 $mL.min^{-1}$, an automatic injector (SIL-20A, Shimadzu, Japan) set-up at 500 μL, a 0.45 μm guard filter unit, an analytic size-exclusion column OHpak SB 807 HQ with a guard column OHpak SB-G (Shodex™, Showa Denko America, Inc., NY, USA), and three detectors: (i) a multiangle light scattering detector (Dawn® EOS, Wyatt Technology Corp., Santa Barbara, CA, USA) fitted with a K5 cell of 50 μL, a 5 mW red source (Ga-As 690 nm) and 18 diodes, (ii) a differential refractive index detector (RID-10A, Shimadzu, Japan), and (iii) a differential viscosimeter detector (Viscostar II, Wyatt Technology Corp., Santa Barbara, CA, USA). The eluent solvent (0.1 M $LiNO_3$) was filtered through a 0.1 μm filter unit. The differential refractive index dn/dC value was 0.15 $mL.g^{-1}$. Data were analyzed on Astra v6.0.6.13 software (Wyatt Technology Corp., Santa Barbara, CA, USA).

2.5. Preparation of HA liposomal mixtures for SANS experiments

HA solution was prepared by dissolving HA powder in D_2O buffer (HEPES/NaCl 10/115 mM, pH 7.4). HA-liposome mixtures (HA-Lip, HA-Lip^+, HA-Lip^-, HA-Lip PEG, and HA-DexP-LipPEG) were prepared by dissolving HA at 1.5% (w/v) in liposome suspensions at 80 mM of lipid concentration. HA solutions and HA-liposome mixtures were immediately homogenized by vortexing for 10 min, maintained at room temperature for 1 h, and manually stirred for 30 s. Bubbles were removed using a vacuum pump, and samples were kept at 4 °C for at least 12 h before use. HA-Lip PEG mixtures (80 mM lipids) were also prepared at 0.15% (w/v) of HA to evaluate the effect of the HA concentration on liposomal mixture behavior.

2.6. SANS

SANS experiments were carried out on the PAXY instrument at Laboratoire Leon Brillouin (Saclay, France). q is the modulus of the scattering vector ($q = (4\pi/\lambda)\sin\theta$) with 2θ the scattering angle. To cover a q-range from 0.002 to 0.5 $Å^{-1}$, four configurations were used with the following wavelengths λ and sample-detector positions D (λ = 5 Å, D = 1 m; λ = 5 Å, D = 3.5 m; λ = 8 Å, D = 5 m; λ = 15 Å, D = 7 m). Liposomal suspensions and liquid formulations were measured in 1 mm-path length rectangular quartz Hellma cells. Viscous mixtures at 1.5% HA (w/v) were included in homemade quartz cells manufactured at Laboratoire Leon Brillouin. The mixture was contained between two cylindrical slices (diameter = 10 mm, thickness = 1 mm) separated by a 1 mm spacer. Then, it was trapped in a homemade measurement cell to prevent sample evaporation. All samples were thermostated at 37 °C through a circulation water bath system. Data were corrected from the electronic background and empty cell. They were normalized to absolute scale (cm^{-1}) using standard procedures implemented in PAsiNET software at Laboratoire Leon Brillouin.

2.7. SANS data analysis

The scattering intensity I(q) from suspensions exhibiting a vesicle shape was defined as:

$$I(q) = \phi_{lipids} \times \left(\rho_{solv} - \rho_s\right)^2 \times V_{tot} \times P(q) \times S(q) + I_{bck} \qquad \text{Eq. 3}$$

with ϕ_{lipids} the volume fraction of lipids, ρ_s and ρ_{solv} respectively the scattering length densities of the shell (lipid bilayer) and the solvent (whom difference is the contrast), V_{tot} the total volume of the vesicle. *P(q)* is the form factor that gives information on the particle size and shape, *S(q)* the structure factor that gives correlations between centers of mass of vesicles, and is thus directly linked to inter-particle interactions, and I_{bck} is the contribution of the background signal (due for example to incoherent scattering in the case of neutrons). Polydispersity was applied to the core and the shell independently, assuming a gaussian and a lognormal distribution, respectively. The diameters $2R_N$ of the vesicles (without HA) were calculated from the parameter values extrapolated from the best fits of SANS data with the formula $2R_N = 2R_c + 2t_{s\,(N)}$ with R_c the core radius and $t_{s\,(N)}$ the shell thickness. The aggregation number of liposomes N_{agg} was estimated as follows:

$$I(q=0) = N_{agg} \times V_{tot}{}^2 \times \phi_{lipids} \times \left(\rho_{solv} - \rho_s\right)^2 \times P(q=0) \quad \text{Eq. 4}$$

The gyration radius R_G of the vesicles was extrapolated from the Guinier plot (*see supplementary material,* Fig. S1). The scattering intensity from dexamethasone phosphate aggregates was modelled with a sphere model for the form factor and a Hayter-Penfold for the structure factor *(see supplementary material).* A unilamellar vesicle model with a hard-sphere structure factor *(see supplementary material)* was used to fit the curve from DexP-LipPEG suspension.

In SANS experiments, neither unilamellar nor multilamellar vesicle models described adequately Lip suspension data (*see supplementary material*, Fig. S3). So, the scattering intensity I(q) from a lamellar phase was also used for this system:

$$I(q) = \phi_{lipids} \times \left(\rho_{solv} - \rho_L\right)^2 \times \frac{2\pi P(q)}{q^2 t_L} + I_{bck} \quad \text{Eq. 5}$$

with t_L the total layer thickness. Form factors were detailed in the supplementary material.

3. Results

First, we characterized the individual components of the system (*i.e.* liposomes and HA solution) by using different methods (DLS, cryo-EM, and SANS for liposomes and SEC, viscometry, and SANS for HA) before studying hybrid systems (*i.e.* HA-liposomes mixtures) by SANS. SANS experiments were conducted at 37 °C to be close to physiological conditions in a HEPES/NaCl buffer (10/115 mM, pH 7.4) mimicking biological fluids.

3.1. Liposome characterization

Liposomes of different surface properties were prepared: neutral (Lip), cationic (Lip^+), anionic (Lip^-), and PEGylated (LipPEG). Their size, polydispersity, and surface characteristics are presented in Table 2.

Table 2. Size and surface characteristics of liposome suspensions, determined by DLS, cryo-EM, and SANS. D_h: hydrodynamic diameter determined by DLS; D_{EM}: liposome diameter, $t_{s\,(EM)}$ shell thickness, and N_s: mean number of shells determined by cryo-EM; $2R_N$: liposome diameter and $t_{s\,(N)}$: shell thickness calculated from the parameter values obtained for the best fit of SANS data with a vesicle model; $2R_G$: liposome diameter extrapolated from Guinier radius R_G obtained from SANS.

Name *Lipid composition*	**Electrophoretic mobility/DLS** *25 °C, [Lipids] = 2 mM*			**Cryo–EM**			**SANS** *37 °C, [Lipids] = 80 mM*		
Lipid ratio (mol%)	ζ potential (mV)	D_h by intensity (nm)*	D_h by number (nm)	D_{EM} (nm)*	$t_{s\,(EM)}$ (nm)*	N_s *	$2R_N$ (nm)*	$t_{s\,(N)}$ (nm)*	$2R_G$ (nm)
Lip *EPC:Chol 65:35*	–10 ± 1	85 ± 17 [0.13]	68 ± 12	82 ± 41 [0.25]	4.5 ± 0.5 [0.02]	1.9 [0.44]	*n.d.*	*n.d.*	52
Lip$^+$ *EPC:Chol:SA 55:35:10*	+53 ± 3	82 ± 13 [0.10]	67 ± 23	73 ± 32 [0.19]	5.5 ± 0.5 [0.01]	1.2 [0.14]	36 ± 7 [0.22]	3.9 ± 0.4 [0.11]	40
Lip$^-$ *EPC:Chol:PG 55:35:10*	–56 ± 4	72 ± 11 [0.09]	58 ± 10	56 ± 32 [0.33]	5.4 ± 0.4 [0.01]	1.1 [0.05]	32 ± 6 [0.20]	3.7 ± 0.5 [0.13]	42
LipPEG *EPC:Chol:DSPE-PEG$_{2000}$ 60:35:5*	–43 ± 5	78 ± 15 [0.15]	65 ± 21	52 ± 27 [0.27]	4.8 ± 0.6 [0.01]	1.1 [0.06]	32 ± 6 [0.20]	3.9 ± 0.5 [0.13]	36
DexP-LipPEG *EPC:Chol: DSPE-PEG$_{2000}$ 60:35:5*	–36 ± 1	83 ± 13 [0.09]	69 ± 22	*n.d.*	*n.d.*	*n.d.*	50 ± 9 [0.21]	*n.d.*	62

*The corresponding polydispersity index or polydispersity ratio value is reported in brackets. *n.d.*: not determined

The different liposomes were characterized by a monodisperse distribution by intensity of D_h (DLS) of around 80 nm, whatever their charge and nature. The measured size was different depending on the technic used. Larger diameters were measured by DLS, followed by those determined by cryo-EM (Table 2). When liposome distribution by DLS was expressed by number, namely by rectifying the distribution from the scattering of the largest particles, D_h was decreased by 15 nm and closer to D_{EM}. Cryo-EM images showed that liposomes were unilamellar except for Lip, which were oligomellar (Fig. 1).

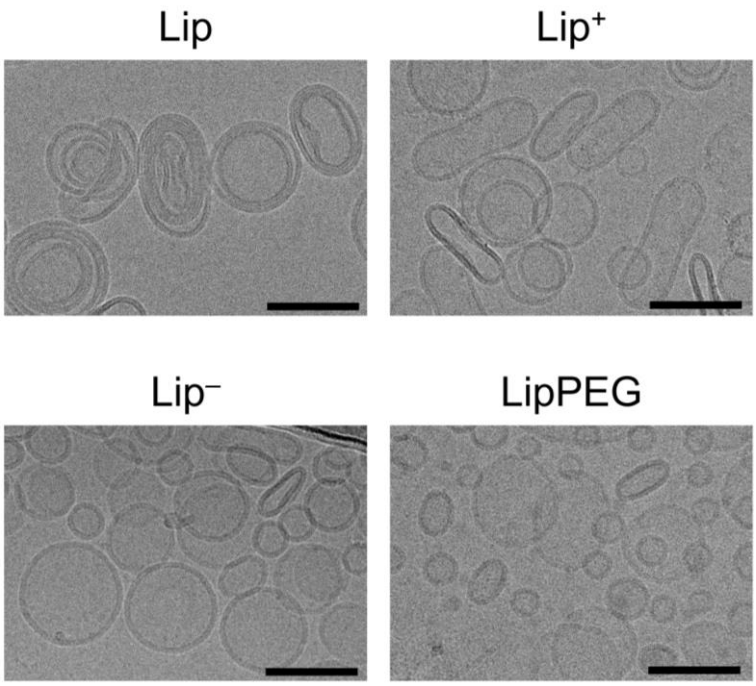

Fig. 1. Cryo-EM images of liposome suspensions in D_2O buffer (HEPES/NaCl 10/115 mM, pH 7.4). Scale bar = 100 nm.

3.1.1. SANS experiments: effect of liposome surface

SANS curves of liposome suspensions at 80 mM in D_2O buffer HEPES/NaCl are shown in Fig. 2, with their respective fitting.

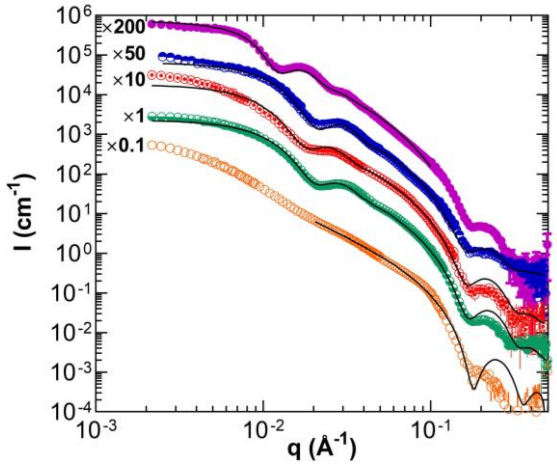

Fig. 2. Scattering intensity from liposome suspensions. Bests fits of form factors from SANS data analysis are represented in full lines. Lip (○), Lip^+ (⊙), Lip^- (◒), LipPEG (◓), DexP-LipPEG (●). [Lipids] = 80 mM, T = 37 °C, D_2O buffer (HEPES/NaCl 10/115 mM, pH 7.4).

The SANS data were fitted by pure form factors P(q). A lamellar model better adjusted the scattered intensity of Lip (*see supplementary material*, Table S1) while Lip^+, Lip^- and LipPEG were fitted by a unilamellar vesicle model (parameters are presented in Table 3).

Table 3. Fit parameters from SANS data analysis to a unilamellar vesicle model for the form factor. [Lipids] = 80 mM, T = 37 °C, D_2O buffer (HEPES/NaCl 10/115 mM, pH 7.4). Theoretical ϕ_{lipids}: theoretical volume fraction of the lipids; R_c: core radius; t_s: shell thickness; ρ_s, ρ_{solv}: scattering densities of the shell and solvent.

Suspensions:	**Lip^+**	**Lip^-**	**LipPEG**	**DexP-LipPEG**
Theoretical ϕ_{lipids}	0.048	0.051	0.051	0.051
R_c (nm)*	14 [0.22]	12 [0.20]	12 [0.19]	21 [0.21]
t_s (nm)*	3.9 [0.11]	3.7 [0.13]	3.9 [0.13]	–
ρ_s (10^{-6} Å^{-2})	0.19	0.24	0.22	0.22
ρ_{solv} (10^{-6} Å^{-2})	6.33	6.33	6.33	6.33

*The corresponding polydispersity ratio value is reported in brackets.

Aggregation numbers N_{agg} were estimated by dividing the experimental intensity $I(q)_{q\to0}$ by the fitted one at q = 0. Relatively low values (N_{agg} ~1–2) were obtained. It allowed determining $2R_N$ and $2R_G$ liposome diameters from these concentrated suspensions (Lip^+, Lip^- and LipPEG). The $2R_N$ diameter was around 32–36 nm, and the thickness of the shell (lipid bilayer) around 3.7–3.9 nm (Table 2). However, the gyration radius R_G seemed closer to cryo-EM values than R_N radius (Table 2) and thus more representative of the sample. Overall, the size of the different kinds of liposomes was similar by SANS analysis. However, the actual size of LipPEG might be slightly higher than the one observed by SANS due to the PEG_{2000} corona being organized in brush (~4.5 nm) [22]. Indeed, the PEG layer was almost invisible to neutrons for contrast reasons due to its hydration by the D_2O solvent.

For neutral liposomes (Lip), the SANS curve was not adequately fitted by the unilamellar vesicle model because no oscillation was observed in the intermediate q-range. As the cryo-EM images suggested deformed oligolamellar liposomes (Fig. 1), we also tested a multilamellar vesicle model (see *supplementary material*, Fig. S3). It was not able to fit the data at intermediate q. The presence of a q^{-2} variation over a large q-range at intermediate q was better described by a lamellar model (Table S1). Although this latter model was not suited to depict the actual sample or fit low q data, this approach allowed to determine the thickness of the lipid bilayer, which was equivalent to that of the other liposome suspensions (t_L = 3.7 nm). The

presence of a poorly defined oscillation around q = 0.006 $Å^{-1}$ suggested a high polydispersity in the number of bilayers and/or in the inter-bilayer distance. It is in accordance with the cryo-EM images (Fig. 1) on which Lip were oligolamellar vesicles with N_s = 1.9. As the correlation function of Lip by DLS was well fitted by a monodispersed distribution (*see supplementary material*, Fig. S2), it is in favor of a large polydispersity of the inter-bilayer distance.

3.1.2. SANS experiments: dexamethasone phosphate-loaded liposomes

Dexamethasone phosphate is a hydrophilic drug that self-associates in water for a concentration superior to the critical aggregation concentration (3.5 mg/mL at 37 °C) [23]. Its molecular structure (*see supplementary material*, Fig. S3) is close to bile salts, which were more extensively studied by SANS [24]. The analysis of SANS data of the dexamethasone phosphate solution (100 mg/mL) used for encapsulation showed small aggregates of 1.7-nm diameter (Table S3). Its scattering had thus a much lower intensity than vesicles at intermediate and low q. The encapsulated drug might impact neutron scattering profiles of liposomes only for q > 0.1 $Å^{-1}$.

DexP-LipPEG suspensions were fitted by a unilamellar vesicle model with a hard sphere structure factor for q < 0.1 $Å^{-1}$. There was a significant increase of the size measured by SANS for DexP-LipPEG compared to LipPEG, as revealed by the shift of the first oscillation of P(q) towards low q. DexP-LipPEG liposomes were enlarged by 20 nm due to the presence of dexamethasone phosphate aggregates in the aqueous core. However, the D_h value measured by DLS was similar between loaded and unloaded LipPEG (Table 2). Besides, if LipPEG without dexamethasone phosphate were slightly aggregated (Fig. 2), it was not the case for DexP-LipPEG for which repulsive interactions appeared.

3.2. Hyaluronic acid characterization

As a semi-rigid polyelectrolyte, the molecular organization of HA in an aqueous medium depends on its concentration and solvent ionic strength. In the present study, the salt concentration of the buffer screened the repulsive electrostatic charges between HA chains (I = 0.115 M). As regards its conformation, HA behaved as a neutral polymer in good solvent conditions [25] while remaining negatively charged. Thus, the organization of HA chains relies mainly on its concentration and can be divided into three domains: the dilute regime, the semi-dilute unentangled and the semi-dilute entangled regimes, delimited respectively by the overlap concentration C^*, and the entanglement concentration C_e. For a weight average molar mass of 1.14 10^6 g/mol determined by size exclusion chromatography coupled on-line with multiangle

light scattering (Table 4), C^* was estimated by extrapolation at a specific viscosity for $\eta_{sp} = 2$ (*see supplementary material,* Fig. S4, C^* ~0.045% w/v) [25]. The R_G value of HA was then around 100 nm according to the following equation [14]:

$$C^* \cong \frac{M_w}{\frac{4}{3}\pi R_G{}^3 N_A} \qquad \text{Eq. 6}$$

with N_A the Avogadro constant. The entanglement concentration $C_e = 0.25\%$ w/v was determined by measuring the specific viscosity as a function of HA concentration in D_2O buffer at 37 °C (*see supplementary material,* Fig. S4).

Table 4. HA characteristics: number average molecular weight (M_n), mass average molecular weight (M_w), polydispersity index (Đ), degree of polymerization and mass average intrinsic viscosity ($[\eta]_w$) determined by size-exclusion chromatography coupled on-line with multiangle light scattering, degree of polymerization, overlap concentration (C^*), and gyration radius (R_G).

M_n (10^6 g/mol)	M_w (10^6 g/mol)	Đ	Degree of polymerization	$[\eta]_w$ (mL/g)	C^* (% w/v)	R_G (nm)
1.00 ±0.03	1.14 ± 0.05	1.13 ± 0.06	2842	1695	0.045	100

HA concentrations of 0.15 and 1.5% w/v belonged to the semi-dilute unentangled and semi-dilute entangled regimes, respectively.

3.3. SANS experiments on HA liposomal mixtures

As the size of all types of liposomes was approximately the same, it was possible to evaluate precisely the influence of their surface on the scattered intensity from HA-liposome mixtures. Then, the effects of HA concentration and drug encapsulation on the scattered intensity were studied for the HA-LipPEG system.

3.3.1. Effect of liposome surface

Mixtures of HA at 1.5% w/v and liposomal suspensions at 80 mM (Lip, Lip^+, Lip^- and LipPEG) were evaluated by SANS at 37 °C (Fig. 3).

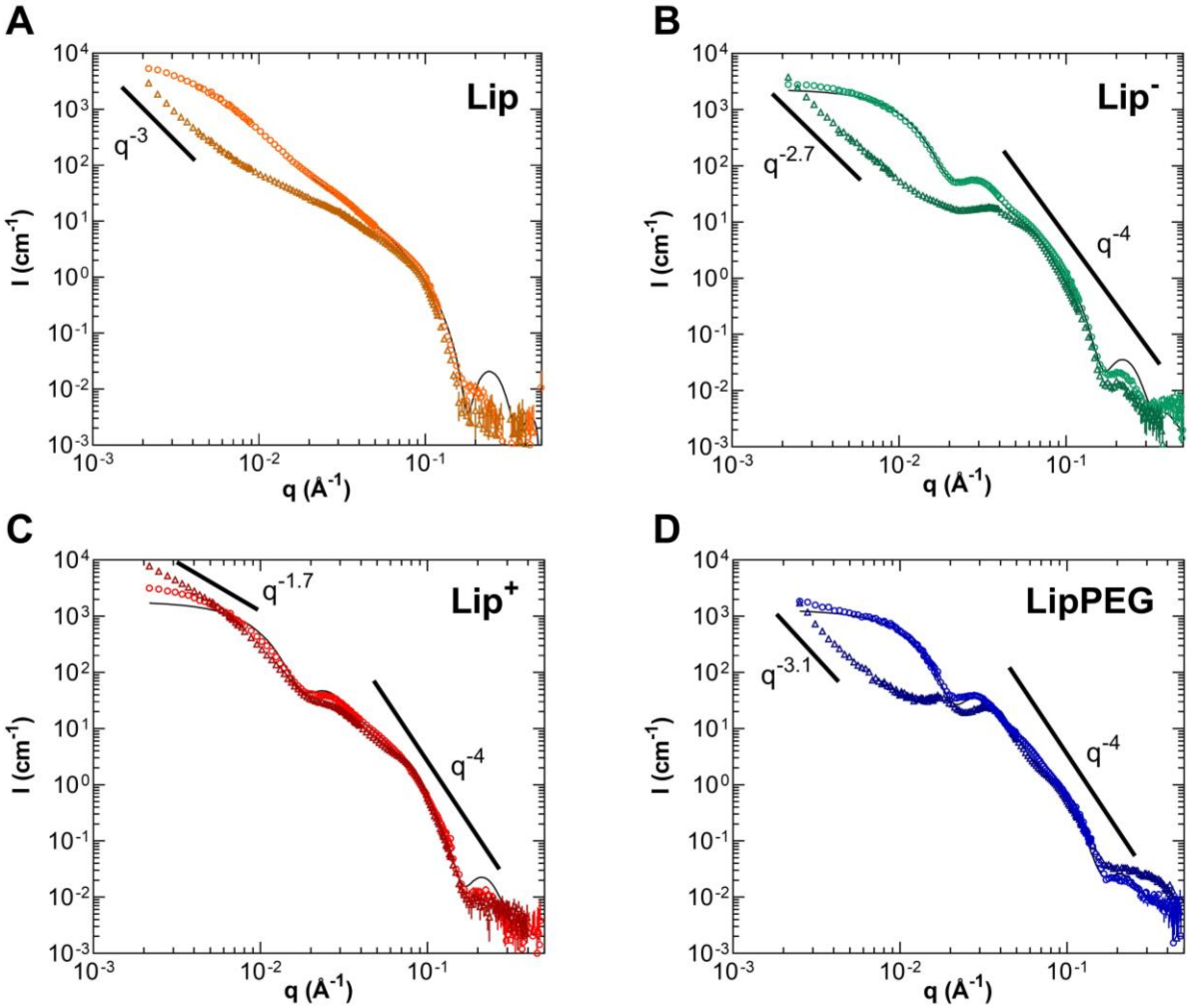

Fig. 3. Impact of liposome surface on scattering intensity for liposomes in suspensions (○) and HA-liposome mixtures (△) with Lip in orange, Lip^+ in red, Lip^- in green, and LipPEG in blue. [Lipids] = 80 mM, T = 37 °C, [HA] = 1.5% w/v in HA-liposome mixtures, D_2O buffer (HEPES/NaCl 10/115 mM, pH 7.4). Bests fits of form factors from SANS data analysis are represented in full lines.

No macroscopic phase separation was observed at this HA concentration regardless of the liposome type. For these hybrid systems, HA contributed significantly to the scattered signal at large angles ($q > 0.1$ Å^{-1}) (*see supplementary material*, Fig. S5). At low q, the scattered intensity was dominated by the scattering of the vesicles.

The curves of HA-Lip, HA-Lip^- and HA-LipPEG were characterized by a sharp rise at low q with a q^{-3} slope (Fig. 3). This slope revealed large density fluctuations within the mixtures, between HA and liposomes. It suggested aggregation of the liposomes, with aggregates larger than the ones that could be probed within the q-range of the SANS experiment. For HA-Lip^- and HA-LipPEG, pronounced correlation peaks appeared at intermediate q that partially

overlapped with the oscillations of the vesicles form factor. Conversely, HA-Lip did not present any correlation peak at intermediate q. This effect might result from the high polydispersity of the objects observed.

For HA-Lip$^+$, the slope at low q was weaker ($q^{-1.7}$) than one of the other liposomes (q^{-3}), suggesting that density fluctuations were less pronounced for this system. A correlation peak was also observed at intermediate q for HA-Lip$^+$ but was much less intense than HA-Lip$^-$ and HA-LipPEG.

Whatever the liposome surface, the scattered intensity at large q for $q > 0.15$ Å^{-1} was strongly influenced by the presence of HA compared to those of pure liposomes. The polymer was responsible for the differences in the profile. However, the curves were almost superimposed between 0.07 and 0.15 Å^{-1} (Fig. 3). In the case of Lip$^+$, Lip$^-$ and LipPEG (fitted by a vesicle model), the q-position of the oscillation arising from the bilayer's thickness at the edge of the q^{-4} decay at high q was similar for both suspensions and HA-liposome mixtures. It means that the thickness of the lipid bilayer is unchanged, and the form of the vesicles is not drastically modified, even if liposomes might have been slightly distorted.

Since the shape of the vesicles was not modified in the presence of HA or only weakly changed, it appeared that the correlation peaks at intermediate q arose from correlations between the vesicles. In all cases, the position of the second correlation peak was observed precisely at twice the position of the correlation peak q_0, *i.e.* it was its harmonics. It allowed the calculation of a center-to-center distance between two vesicles, the so-called d-spacing d_0 in direct space, from $d_0 = 2\pi/q_0$ (Table 5).

Table 5. Structure factor characteristics of HA-liposome mixtures, assuming liposomes retained their vesicular shape and size in HA solutions. [Lipids] = 80 mM, T = 37 °C, [HA] = 1.5% w/v, D_2O buffer (HEPES/NaCl 10/115 mM, pH 7.4). q_0: length of the scattering vector at the lower correlation peak; d_0: d-spacing between two vesicles or characteristic length of the system.

HA-liposome mixtures	q_0 (Å^{-1})	d_0 (nm)	Harmonics
HA-Lip$^+$	0.0175	35.9	$1q_0$, $2q_0$
HA-Lip$^-$	0.0204	30.8	$1q_0$, $2q_0$
HA-LipPEG	0.0212	29.6	$1q_0$, $2q_0$
HA-DexP-LipPEG	0.0124	50.7	$1q_0$, $2q_0$

These distances correlate well with the corresponding $2R_N$ diameter of the liposomes (Table 2). It shows that liposomes were in close contact within the HA network.

3.3.2. Effect of HA concentration

We assessed the impact of HA concentration on the scattered intensity profile of HA-LipPEG mixtures when HA was in the semi-dilute unentangled regime. It prompted us to choose a concentration of 0.15% w/v (Fig. 4).

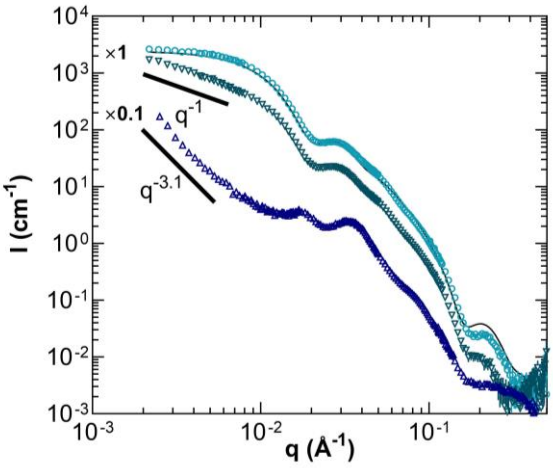

Fig. 4. Scattering intensity of LipPEG in suspensions (○), in HA solution at 0.15% w/v (▽, $C^* < C < C_e$) or at 1.5% w/v (△, $C > C_e$). T = 37 °C, [Lipids] = 80 mM, D_2O buffer (HEPES/NaCl 10/115 mM, pH 7.4).

At this concentration, the viscosity of the medium was low (sampling with pipette was possible). The decay of the scattered intensity at low q (q^{-1}) was much lower than at 1.5% w/v ($q^{-3.1}$). At 0.15%, HA chains were not entangled, while at 1.5%, they formed a network. The fact that HA formed a network at 1.5% seemed to increase density fluctuations drastically in

the hybrid system. Despite the high lipid concentration (80 mM) used for HA-LipPEG mixtures and LipPEG suspension, the lipid volume fraction appeared lower in HA-LipPEG at 0.15% w/v HA than the LipPEG suspension in SANS data (Fig. 4). Due to the lower viscosity, a slight creaming was observed during the experiment; thus, the neutron beam might have crossed the sample in the most diluted part of the sample.

3.3.3. Effect of HA on dexamethasone phosphate-loaded liposomes

As demonstrated in section 3.1.2, the encapsulation of a hydrophilic drug such as dexamethasone phosphate significantly increased LipPEG size (SANS). Surprisingly, there was no shift of the correlation peaks towards smaller angles for the HA-DexP-LipPEG compared to HA-LipPEG (Fig. 5).

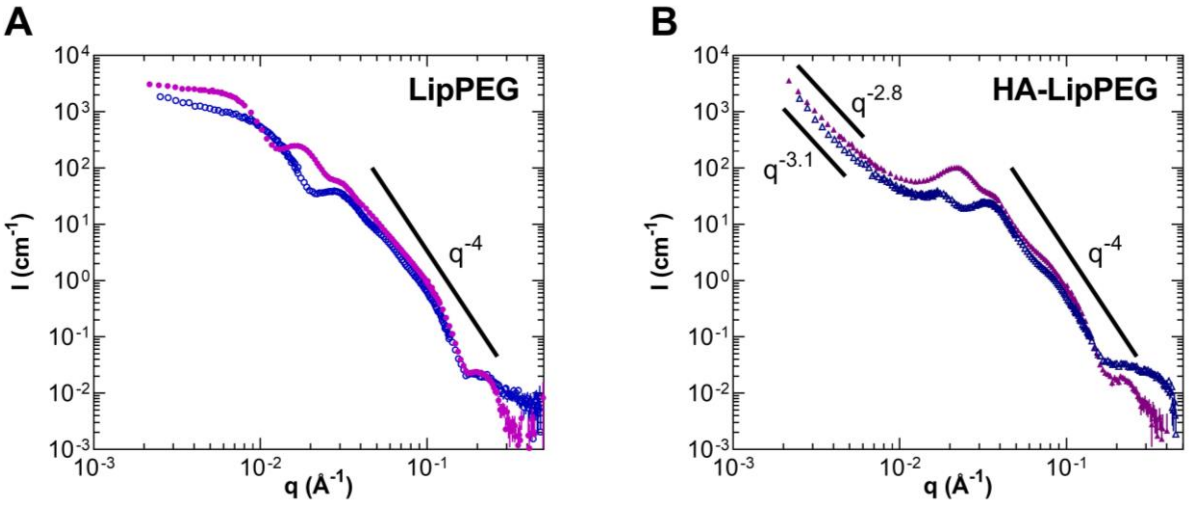

Fig. 5. Effect of dexamethasone phosphate encapsulation within LipPEG on the scattering intensity. **(A)** LipPEG (○) and DexP-LipPEG (●) suspensions. **(B)** HA-LipPEG (△) and HA-DexP-LipPEG (▲). [Lipids] = 80 mM, T = 37 °C, [HA] = 1.5% w/v in HA-liposome mixtures, D_2O buffer (HEPES/NaCl 10/115 mM, pH 7.4).

As in the previous section, the position of the second correlation peak was precisely at twice the position of q_0 (Table 5). The resulting d-spacing d_0 between the centers of two vesicles corresponded exactly to $2R_N$ diameter within the HA-DexP-LipPEG mixture. When the LipPEG size was enlarged by 20 nm, due to dexamethasone phosphate encapsulation, the d-spacing d_0 was increased by the same distance. Furthermore, for both HA-LipPEG mixtures with or without dexamethasone phosphate, a slope in $\sim q^{-3}$ was observed at low q meaning that the presence of dexamethasone phosphate did not modify the heterogenous organization of the system.

4. Discussion

In the pharmaceutical field, HA-liposome mixtures is a versatile hybrid system suitable for different administration routes such as the transtympanic one [6]. They showed many advantages for sustained drug delivery. Before considering their clinical use, it is crucial to understand the physicochemical properties of these systems to control their use properties. Thus, the main objective of this work was to elucidate the impact of HA concentration, liposome surface and drug encapsulation on the organization and structure of liposomes within the hybrid system. We first characterized the liposomal suspensions by SANS, DLS and cryo–EM. Then, we explored the HA-liposomes systems by SANS. Different parameters were studied: HA concentration ($C^* < C < C_e$ and $C > C_e$), the liposome surface and dexamethasone phosphate encapsulation.

The size characteristics of Lip^+, Lip^- and LipPEG were consistent with the literature (for review, see [26]). Only Lip seemed to exhibit a polydisperse internal structure, as confirmed by cryo–EM images (Fig. 1), and were therefore not fitted with a vesicle model. The size measured by SANS was lower than that of cryo-EM and DLS. DLS measurements determine a correlation time related to a diffusion coefficient of the colloidal objects and then to a hydrodynamic diameter through the Stokes-Einstein equation. D_h takes into account the hydration layer surrounding the colloids. Conversely, SANS provides a structural determination. Neutrons are scattered by the nuclei of the atoms of the objects. The difference of scattering length density between the deuterated buffer and the protonated phospholipids dominates the scattering length density profile of the liposomes. The hydration shell thickness is not taken into account. Both methods (SANS and DLS) detect an ensemble of particles whereas cryo-EM measures the size of single particles. In this latter technic, the image reflects the electron density inhomogeneities within the sample. The measured diameter is thus closer to the core size than to hydrodynamic diameter. These discrepancies were observed experimentally and also reported by Varga et al [27]. Furthermore, DLS was performed on diluted samples (2 mM) in milliQ water, which may favor an osmotic pressure-driven increase of liposome size.

Interestingly, when dexamethasone phosphate was encapsulated into LipPEG, the vesicles were enlarged by 20 nm according to SANS results, which was not expected. Indeed, such a difference in size was not observed by DLS. The origin of this upsizing is not explained yet, though it might be induced by a difference in the ionic strength inside and outside the vesicles. However, the osmolarities inside and outside the DexLipPEG were of the same order

(~300 mOsm/kg). The lack of investigation for hydrophilic compound encapsulation within vesicles in the SANS literature did not allow any comparison. Most of the publications studied drug encapsulation within the lipid bilayer (for review, see Di Cola et al. (2016)). The signature of the DexP micelles for q > 0.1 $Å^{-1}$ is still observed in the SANS profile of the liposomes (Fig 5), indicating that most DexP molecules are in the aqueous compartment of the vesicles. We do not exclude that some DexP molecules could also be embedded in the lipid bilayer of the liposomes due to their amphiphilic character. However, this insertion in the bilayer is likely to be limited. Indeed, we did not observe a significant modification of the Zeta potential value (–43 ± 5 mV without DexP *versus* –36 ± 1 mV with DexP, (see Table 2). In addition, even if we did not fit the large q data of the DexLipPEG (the remaining scattering of DexP in solution in such q-regime would had introduced a large uncertainty on the value obtained for the bilayer thickness), the SANS oscillation related to the phospholipid bilayer was not qualitatively influenced by DexP. It means this drug does not modify the lipid bilayer characteristics (thickness and polydispersity).

Besides the increase of vesicle size, the presence of a negatively charged cargo (dexamethasone phosphate) seemed to induce an additional repulsion between the DexP-LipPEG. Surprisingly, this behavior observed by SANS did not reflect on ζ potential values (Table 2).

In a second step, we assessed the influence of HA on the SANS profiles of the different suspensions in the high salt limit since HA was dissolved in a buffer mimicking biological fluids (HEPES/NaCl, 10/115 mM, pH 7.4). Two HA concentrations were chosen, 0.15% and 1.5%, in the semi-dilute unentangled and entangled regimes, respectively. The low intensity of the HA signal measured by SANS at low q (*see supplementary material*,Fig. S6) did not allow us to determine the mesh size ξ of the network at 1.5% w/v experimentally. However, we could estimate its value. Assuming that HA was in the high salt limit in good solvent conditions, the correlation length scales with HA concentration as follows [14]:

$$\xi \cong R_G \left(\frac{C^*}{C} \right)^{3/4} \qquad \text{Eq. 7}$$

The correlation length ξ was thus estimated at ~41 nm and ~7 nm respectively for 0.15 and 1.5% w/v of HA. Studies performed with HA of different molecular weights and different concentrations determined mesh sizes between 13 and 22 nm by FRAP technique (1.4–2.4% w/v, M_w = 0.7 10^6 g/mol, saline phosphate buffer, pH 7.3) [28] and ~9 nm by electron

spin resonance technique (1.4% w/v, M_w = 1.01 10^6 g/mol, HEPES/NaCl 50/100 mM, pH 7) [29].

For our polymer-colloid mixtures, the scattering intensity was dominated by the signal of liposomes at low and intermediate q. Thus, it gave direct information on the form factor and the dispersion state of the liposomes within HA. The main results of the study can be summarized as follows:

(1) Whatever the content or surface of the liposomes, they kept their integrity within the HA-liposomes mixtures in the entangled semi-dilute regime (1.5%).

(2) By tuning the liposome surface, their organization was modified within HA solutions in the concentrated regime (1.5%). Anionic liposomes (Lip^- and LipPEG) were in close contact within the mixtures, with a center-to-center distance corresponding to twice the liposome size. In contrast, Lip^+ were less impacted by the presence of HA and appeared more dispersed within the hybrid system than the other ones. With neutral liposomes (Lip), results were difficult to interpret due to their polydispersity.

(3) The change in the HA concentration regime induced a rearrangement of liposomes within the mixtures. In the semi-dilute unentangled regime, LipPEG were slightly perturbated by the presence of HA at the micro-scale. Conversely, in the concentrated regime, LipPEG were in close contact.

(4) The encapsulation of dexamethasone phosphate enlarged LipPEG size but the vesicles remained in close contact within HA solutions at 1.5%, with a center-to-center distance of $2R_N$.

Whether or not liposomes kept their integrity within HA was an essential question for the use of these hybrid systems in drug delivery. Indeed, liposome disruption would lead to a premature release of the encapsulated drug. Liposome volume fraction and bilayer thickness were both preserved. Thus, liposomes remained intact within HA, and the system can be considered a mixture of polymer and colloids.

In the dilute regime, the ratio $R_G/R_{colloid}$ between the HA gyration radius ($R_G \approx 100$ nm) and the radius of the liposomes measured by SANS ($16 < R_{colloid} < 25$ nm) ranged between 4 and 6, placing HA-liposome mixtures in the protein limit ($R_G/R_{colloid} > 1$) [11]. In the semi-dilute regime investigated in our study, the correlation length ξ fixed the range of interactions within

the system. The size ratio, now defined as $D_{colloid}/\xi$, was close to 1 for [HA] = 0.15% w/v and between 4 and 7 for [HA] = 1.5% w/v. At 0.15%, below C_e, the vesicle size (from 32 to 50 nm) is close to the correlation length $\xi \approx 41$ nm, while at 1.5%, above C_e, their size was larger than the HA mesh size $\xi \approx 7$ nm. HA chains were excluded from vesicle volume, increasing HA concentration locally, which could shrink the network mesh size by 50% [30]. This hypothesis is consistent with the increased viscosity previously observed when liposomes were incorporated in HA [31]. Furthermore, vesicles were more concentrated than other polymer–liposomes hybrid systems reported in the pharmaceutical field [32–34].

Whatever the liposome surface and content, they were gathered in clusters that exceeded the scale of observation of SANS. In our work, we reported a slope close to q^{-3} for most HA-liposome mixtures (HA-Lip, HA-Lip^-, HA-LipPEG, and HA-DexP-LipPEG) (Fig. 3). For a better description of the microstructure of polymer-nanoparticle systems, fractal dimensions were associated with specific micro-scale organization in other studies [35,36]. In mixtures of PEG and silica nanoparticles, Kumar and colleagues suggested that the q^{-4} slope was associated with aggregates of silica nanoparticles of finite size, close from a micro-scale phase separation. They attributed the one approaching 3 (as in our case) to the coexistence of aggregates and individual objects [35,36]. Conversely, for cationic liposomes (Lip^+) clusters of fractal dimension 1.7 were formed within HA by electrostatic attraction between liposomes and HA. Such fractal dimension was typical of diffusion-limited aggregation [37]. Silica nanoparticles dispersed in HA solutions (0.8 %, HA 10^5 g/mol) forming ramified clusters [38], also reported similar fractal dimensions (~1.5-2).

Within the aggregates, liposomes were separated by a center-to-center distance corresponding to the diameter $2R_N$ of the liposomes, whatever their surface or content. Liposomes were touching each other and might eventually be distorted due to their close packing. It agrees with previous freeze-fracture electron microscopy experiments on larger liposomes (150 nm) in which honeycomb structures were identified [31]. However, in the present study, Lip^+ seemed less compacted in the presence of HA and more dispersed within aggregates, which suggested that HA chains might coat Lip^+ by complexation. The manufacturing process might favor this coating. Indeed, HA chains were progressively dissolved under shear into the liposome suspension, promoting the complexation between Lip^+ and HA.

Grillo et al. (2020) reported the formation of clusters characterized by a crystalline microstructure with hybrid systems composed of HA and poloxamer micelles (d_{SANS} = 21 nm).

In the semi-dilute regime at high salt concentration and in the protein limit ($3 < D_{colloid}/\xi < 5$, $C > C^*$), small micellar clusters organized into a face-centered cubic liquid crystalline phase, though poloxamer was poorly concentrated (3 vol%) in the mixture. This crystalline organization was reinforced by increasing HA concentration or molecular weight. This structure is usually observed with pure poloxamer micelles, in salt-free solutions and at concentrations above 15 vol%. In the present work, no crystallization of liposomes was observed, even for liposomes with the same surface as the poloxamer micelles (*i.e.* PEGylated). Although liposomes were closely packed in the presence of HA at 1.5%, they were more deformable, and their size was more polydisperse than those of poloxamer micelles. It could impede the crystallization process. Nevertheless, the structure factor S(q) of HA-Lip$^-$ and HA-LipPEG, calculated by dividing the scattered intensity by the form factor P(q), revealed large and well-defined structure peaks (Table 5) that correspond eventually to an amorphous organization [39].

In earlier work on HA-liposome mixtures (150-nm sized liposomes) [40], HA could impact liposome organization within the mixtures depending on their surface properties at the macro- and micro scales. Indeed, for $C < Ce$, segregative phase separation occurred between HA and liposomes within 48 h at the macro scale except for Lip$^+$. Conversely, all mixtures stayed macroscopically homogenous for $C > C_e$ except for HA-Lip$^+$ which underwent a slight syneresis at 2.28% (M.W. supplier = $1.5\ 10^6$ g/mol). At 2.28% of HA, confocal microscopy [40] and freeze-fracture electron microscopy [31] suggested a micro-phase separation between liposomes and HA within the hybrid systems.

The micro-phase separation reported earlier [40] and the close packing of liposomes observed in our study were consistent with a depletion effect of entropic origin [39]. Polymer segments were excluded from the space between colloids. It led to an unbalanced osmotic pressure difference that pushed colloids together [41]. This depletion effect was characterized by segregative phase separation between a colloid-rich phase and a polymer-rich one. When the polymer concentration was increased, so as the viscosity of the hybrid systems, HA network prevented the macro-phase separation. In our study, the depletion effect was likely to cause the segregative microphase separation for HA-Lip, HA-Lip$^-$ and HA-Lip PEG mixtures. However, the possible interactions between liposomes and HA have to be also considered. Indeed, more complexity emerges when polymer chains are attracted to particle surface since both enthalpy, and entropic effects are involved [42]. Besides depletion attraction, other mechanisms were described: tight particle bridging, steric stabilization (layer of adsorbed polymer), and "tele-bridging" where distinct adsorbed layers coexist with longer range bridging [39,43]. The

Velogol-Thwar theory estimates the effect of the non-uniformity of surface charge on the interaction potential between colloid particles that can be attractive even for particles of the same charges. This potential was used to explain the phase diagram obtained with liposomes with oppositely charged polyelectrolyte where a re-entrant aggregation and phase separation were observed [44–46]. Noteworthy, our systems were more concentrated in both lipids and polymer, HA molecular weight was higher, as well as the charge ratio between the polyelectrolyte and the lipids. Moreover, in our study, the polyelectrolyte was hydrated with the liposome suspension to avoid dilution of the system, whereas the other groups added a polyelectrolyte preexisting solution to the liposome suspension.

Neutral liposomes (Lip) could potentially bind to the hydrophobic regions along the HA chain [47], though the depletion effect seemed to prevail over these interactions. For HA-Lip, it was difficult to draw a clear conclusion on its micro-scale organization. Indeed, weak correlation peaks were observed by SANS due to the polydisperse internal structure of Lip suspension. HA could interact with cationic liposomes (Lip^+) by electrostatic attractions and complexation. Gasperini et al. (2015) demonstrated HA (16 10^3 g/mol) could bridge cationic liposomes together to form dense aggregates. When HA concentration increased between 20 to 80 % w/w, a complete coating of their surface was achieved, leading to a shift of ζ potential from positive to negative values. Cryo-EM and small-angle X-ray scattering showed that cationic liposomes were dispersed within HA solutions [48]. In our work, HA could wrap around Lip^+ increasing their distribution within HA. However, we used a high molecular weight HA that could also build inter-particulate bridges. At our level of knowledge, it was not easy to conclude on the local particle organization for HA-Lip^+. For Lip^- and LipPEG, their negative charge at the surface could provide electrostatic repulsions with the negatively charged carboxylate groups of HA. In addition to the repulsive electrostatic interaction, steric repulsions also occurred between the PEG chains present at the surface of liposomes and HA chains [49]. Therefore, HA was unlikely to adsorb on the surface of these vesicles.

We tried to fit the experimental SANS data with a square-well potential or a sticky hard sphere models, that are raw but used in several studies to model the depletion interaction [8]. However, in our case, they did not agree with the data (*data not shown*). A rigorous analysis of the HA-liposome SANS data would require the calculation of dedicated interaction potentials between HA and liposomes, which was beyond the scope of this study. Potential interactions [9,10] and more recent models [50] would certainly better reflect the physics of these hybrid systems.

Fig. 6 summarizes the different HA-liposome microstructures suggested in this study.

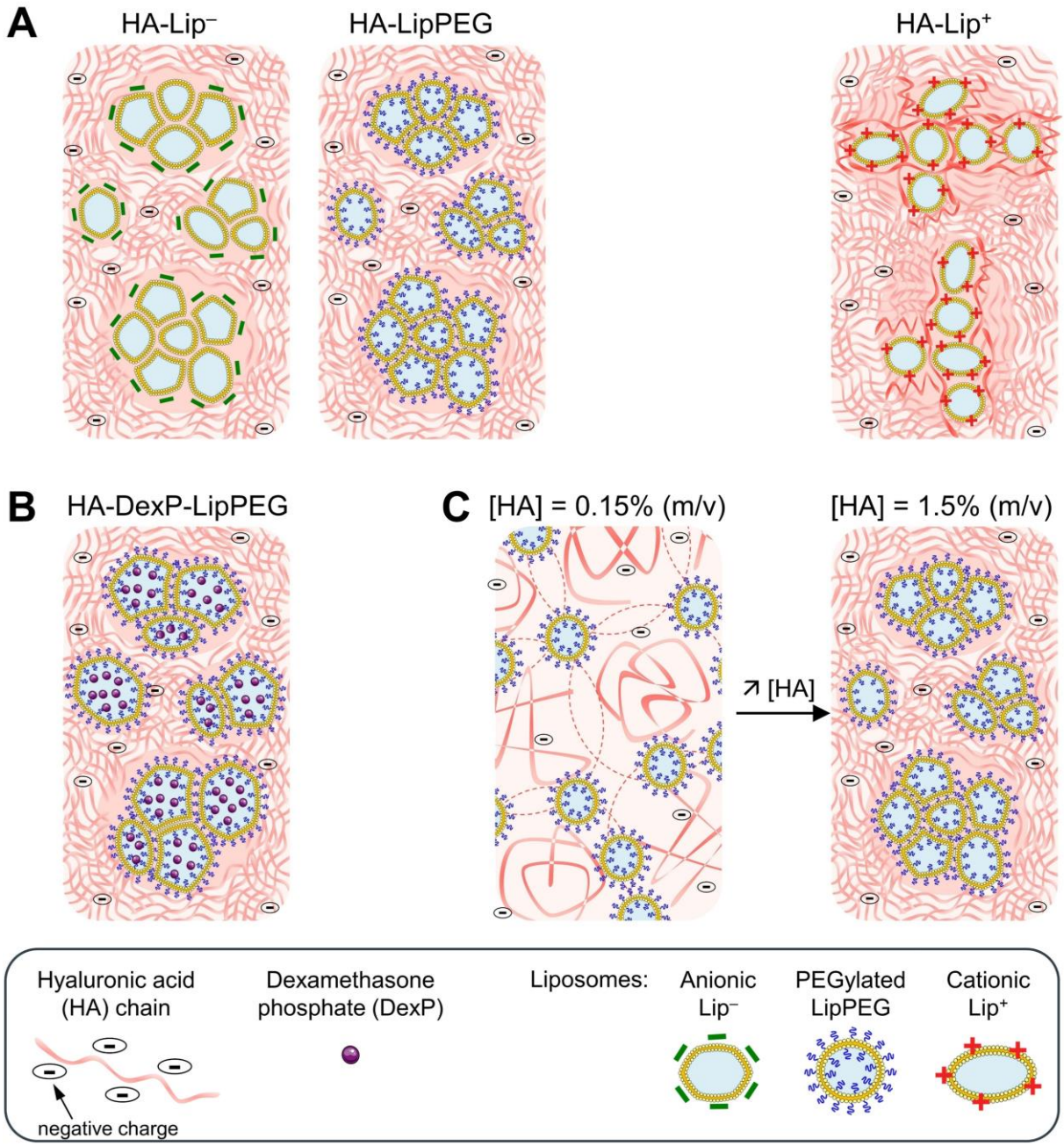

Fig. 6. Schematic representation of the microstructure of HA-liposome mixtures. **(A)** Effect of liposome surface and **(B)** dexamethasone encapsulation within LipPEG on HA-liposome microstructure, [Lipids] = 80 mM, [HA] = 1.5%. **(C)** Effect of HA concentration on LipPEG organization within HA solutions, [Lipids] = 80 mM.

4. Conclusion

This study was performed on complex hybrid systems in the protein limit. Conditions used in this study were particularly relevant for pharmaceutical drug delivery systems (different liposome surfaces and high concentrations of HA and liposomes). SANS proves to be a valuable

tool to characterize their microstructure. It provides information about the internal structure of liposomes in suspensions confirmed by cryo-EM. Except for neutral liposomes, SANS curves of liposome suspensions are adequately fitted by a unilamellar vesicle model. The integrity of all types of liposomes is preserved in HA. In the semi-dilute entangled regime of HA, Lip^- and LipPEG are organized in clusters. They are in close contact in these aggregates, with a center-to-center distance corresponding to twice the liposome size. This result agrees with a depletion mechanism previously reported for mixtures of HA and pluronic micelles [8]. Unlike these micelles, liposomes are in an amorphous organization, probably because they are more deformable and polydisperse. Interestingly, the encapsulation of a drug in the aqueous core of LipPEG does not modify this organization. Due to their complexation with HA, Lip^+ are better disperse within the polymer network. In a further study, we will investigate the impact of these microstructures on the release of liposomes/drugs from these promising and versatile hybrid systems.

Acknowledgements

The authors thank the Laboratoire Léon Brillouin for the beam time on PAXY instrument and Dr. Fabienne Testard (CEA) for her relevant comments on the first draft of the manuscript. Céline Jaudoin acknowledges the Ministère de l'Enseignement Supérieur, de la Recherche et de l'Innovation for her PhD grant 2017-110. This work was supported by ANR (The French National Research Agency) (N° ANR-15-CE19-0014-02). It also benefited from the CryoEM platform of I2BC, financed by the French Infrastructure for Integrated Structural Biology (FRISBI) [ANR-10-INSB-05-05].

CRediT authorship contribution statement

Céline Jaudoin: Conceptualization, Methodology, Investigation, Data curation, Formal analysis, Visualization, Writing – original draft, Writing - review & editing. **Isabelle Grillo:** Conceptualization, Methodology, Investigation, Project administration, Supervision. **Fabrice Cousin:** Investigation, Methodology, Data curation, Formal analysis, Visualization, Writing - review & editing, **Maria Gehrke:** Conceptualization, Methodology, Investigation, Formal analysis. **Malika Ouldali:** Conceptualization, Methodology, Investigation, Review & editing. **Ana-Andreea Arteni:** Conceptualization, Methodology, Investigation, Review & editing. **Luc Picton:** Conceptualization, Methodology, Formal analysis, Review & editing. **Christophe Rihouey:** Conceptualization, Methodology, Formal analysis, Review & editing. **Fanny Simelière:** Methodology, Data curation, Formal analysis, Visualization, Review & editing.

Amélie Bochot: Conceptualization, Project administration, Supervision, Visualization, Writing - review & editing, Funding acquisition. **Florence Agnely**: Conceptualization, Investigation, Project administration, Supervision, Visualization, Writing - review & editing, Funding acquisition

Supplementary material

SANS data supplementary analysis methods

The form factor for a unilamellar vesicle was expressed as follows [51]:

$$P(q) = \frac{\phi_{lipids}}{V_s}\left[\frac{3V_{tot}\, j_1\left(qR_{tot}\right)}{qR_{tot}} - \frac{3V_c\, j_1\left(qR_c\right)}{qR_c}\right]^2 \qquad \text{Eq. S1}$$

where ϕ_{lipids} was the lipid volume fraction, V_s was the volume of the lipidic shell, V_{tot} was the total volume of the vesicle, V_c was the volume of the core, R_{tot} was the outer radius of the shell, R_c was the radius of the core, and j_1 was the spherical bessel function.

The lamellae form factor was [52]:

$$P(q) = \frac{4}{q^2}\sin^2\left(\frac{qt_L}{2}\right) \qquad \text{Eq. S2}$$

The distance δ between two bilayers was calculated as $\frac{2\pi\phi_{lipids}}{t_L}$.

The scattering intensity was expressed as $I(q) = P(q)\times S(q) + I_{bck}$ with $P(q)$ the sphere form factor of dexamethasone phosphate aggregates defined as:

$$P(q) = \frac{\phi_{aggregates}}{V_{sphere}}\times\left[3V_{sphere}\times\left(\rho_{solv}-\rho_{sphere}\right)\times\frac{\sin(qR_c)-qR_c\cos(qR_c)}{\left(qR_c\right)^3}\right]^2 \qquad \text{Eq. S3}$$

with $\phi_{aggregates}$ the volume fraction of the aggregates, R_c and $\rho_{aggregates}$ the core radius and the scattering density of the aggregates. The structure factor $S(q)$ represented interparticle interactions and was calculated using the method of Hayter–Penfold Rescaled Mean Spherical Approximation for charged spheres [53]. The Debye screening length κ^{-1} was calculated as $\left(\frac{8\pi N_{Avogadro}e^2 I}{1000\varepsilon K_B T}\right)^{1/2}$ where I was the ionic strength $= \frac{1}{2}\left(z_{Na^+}\right)^2\left[Na^+\right]$, ε was the dielectric constant of D_2O, K_B was the Boltzmann constant and e was the electronic charge.

The multilamellar vesicle form factor was defined as:

$$I(q) = \frac{\phi_{liposomes}}{V\left(R_N\right)}\times P^2(q) + I_{bck} \qquad \text{Eq. S4}$$

where

$$P(q) = \left(\rho_s - \rho_{solv}\right)\sum_{i=1}^{N}\left[\begin{array}{l} 3V\left(r_i\right)\dfrac{sin\left(qr_i\right) - qr_i\,cos\left(qr_i\right)}{\left(qr_i\right)^3} \\ \\ -3V\left(R_i\right)\dfrac{sin\left(qR_i\right) - qr_i\,cos\left(qR_i\right)}{\left(qR_i\right)^3} \end{array}\right] \qquad \text{Eq. S5}$$

for the solvent radius before shell i: $r_i = R_c + \left(i-1\right)\left(t_L + t_w\right)$ Eq. S6

and the shell radius for shell i: $R_i = r_i + t_L$ Eq. S7

With $\phi_{liposomes}$ the volume fraction of liposomes, $V(r)$ the volume of a sphere of radius r, R_N the outer-most shell radius and t_w the thickness of the solvent layer between the shells.

Liposome characterization by SANS and DLS

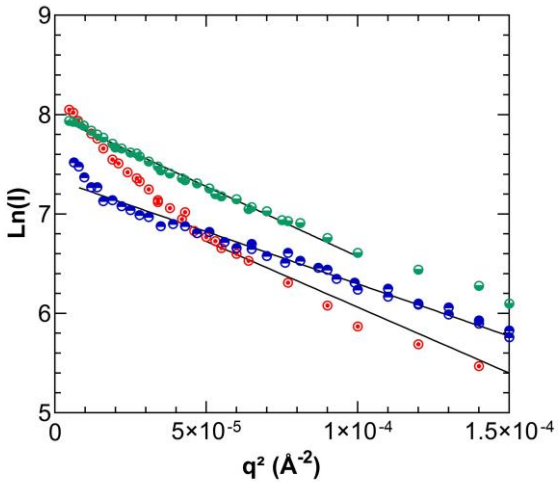

Fig. S1. Guinier representation for Lip⁻ (◒), Lip⁺ (⦿) and LipPEG (◓). T = 37 °C, [Lipids] = 80 mM, D_2O buffer (HEPES/NaCl 10/115 mM, pH 7.4). Full lines correspond to the linear fit at small values of the scattering vector q. The slope was $R_G^2/3$.

Table S1. Fit parameters from the SANS data analysis of Lip to a lyotropic lamellar phase model for the form factor. T = 37 °C, D_2O buffer (HEPES/NaCl 10/115 mM, pH 7.4). ϕ_{lipids} theoretical: theoretical volume fraction of the lipids; t_L: layer thickness; ρ_L, ρ_{solv}: scattering densities of the layer and solvent.

	Lip
[Lipids] (mM)	80
ϕ_{lipids} theoretical	0.051
t_L (nm)*	3.7 [0.05]
Distance between two layers (nm)	71.8
ρ_L (10^{-6} Å^{-2})	0.22
ρ_{solv} (10^{-6} Å^{-2})	6.33

*The corresponding polydispersity ratio value is reported in brackets.

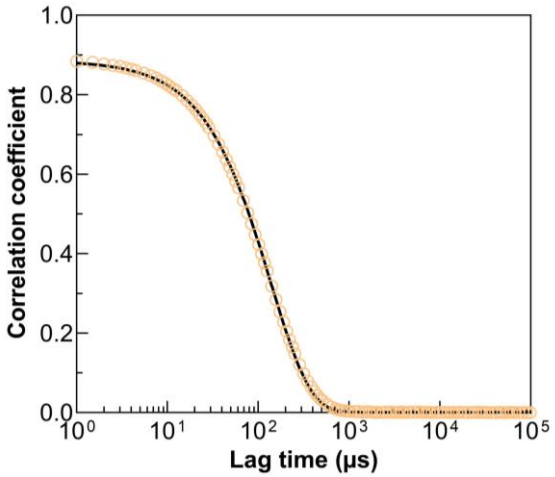

Fig. S2. Correlation coefficient measured by dynamic light scattering as a function of the lag time for Lip (○). Full line represents the best fit for a mono-exponential decay (R^2 = 0.9999).

Table S2. Fit parameters from the SANS data analysis of Lip to a multilamellar vesicle model for the form factor. [Lipids] = 80 mM, T = 37 °C, D_2O buffer (HEPES/NaCl 10/115 mM, pH 7.4). R_c: core radius; N_s: shell number per liposomes; t_s: thickness of the shell; t_w: thickness of the solvent layer between the shells; ρ_s, ρ_{solv}: scattering densities of the shell and solvent.

Suspensions:	**Lip**
R_c (nm)	80 [0.3]
t_s (nm)*	3.5 [0.1]
t_w (nm)* #	9.6 [1.15]
N_s * #	1.9 [0.44]
ρ_s (10^{-6} Å^{-2})	0.22
ρ_{solv} (10^{-6} Å^{-2})	6.33

*The corresponding polydispersity ratio value is reported in brackets. #Measured from cryo–EM images (198 counts).

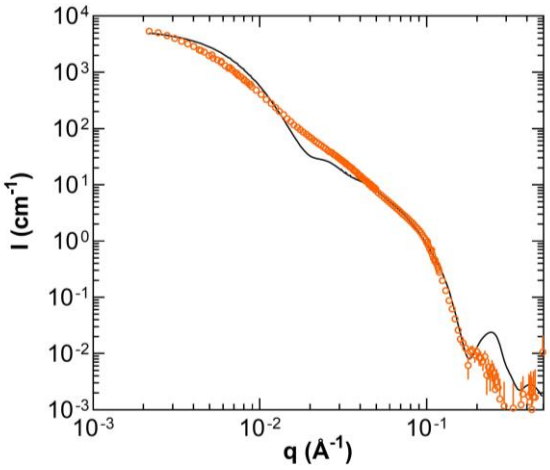

Fig. S3. Scattering intensity for Lip in suspensions (○). [Lipids] = 80 mM, T = 37 °C, D_2O buffer (HEPES/NaCl 10/115 mM, pH 7.4). The best multivesicular fit of Lip form factor from SANS data analysis is represented in full line.

Dexamethasone phosphate micelle characterization by SANS

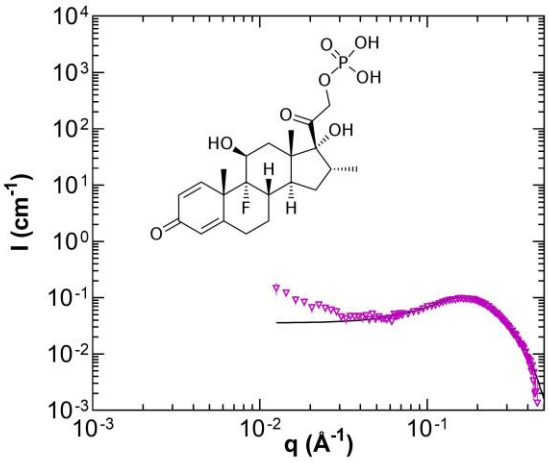

Fig. S4. Scattering intensity from dexamethasone phosphate at 100 mg/mL in D_2O. T = 37°C. The full line represents the best fit from SANS data analysis to a sphere for the form factor and to a Hayter-Penfold rescaled mean spherical approximation for the structure factor.

Table S3. Fit parameters from the SANS data analysis of dexamethasone phosphate in D_2O to a sphere model for the form factor and Hayter-Penfold rescaled mean spherical approximation for the structure factor. T = 37 °C. $\phi_{aggregates}$: volume fraction of the aggregates; R_c: radius of the aggregate core; $\rho_{aggregates}$, ρ_{solv}: scattering densities of the aggregates and solvent; ε: D_2O dielectric constant.

	Dexamethasone phosphate
Concentration (mg/mL)	100
$\phi_{aggregates}$	0.023
R_c (nm)	0.84
Charge of aggregates (e)	–16
$[Na^+]$ (mol/L)	0.39
ρ_{sphere} (10^{-6} Å^{-2})	1.46
ρ_{solv} (10^{-6} Å^{-2})	6.40
ε	74

HA characterization by rheological measurements

Flow measurements were performed in triplicate on HA solutions (0.05, 0.075, 0.1, 0.15, 0.2, 0.25, 0.3, 0.5, 0.7, 1 et 1.5% (w/v)) prepared in D_2O buffer (HEPES/NaCl 10/115 mM, pH 7.4), using a rotational rheometer ARG2 (TA instruments, New castle, USA) equipped with an

aluminum cone/plate geometry (diameter 4 cm, angle 1° and cone truncation 28 μm). After 2 min of equilibration at 37 °C, the shear rate was decreased from 1000 to 0.01 s^{-1} and measurements were performed under steady state conditions.

Below C_e, HA solutions had a Newtonian behavior and the corresponding rheograms were fitted with the Newton equation (Eq. S8) using TRIOS software (TA instruments – Waters LCC, New Castle, USA) to determine the viscosity η that is independent of the shear rate $\dot{\gamma}$ (s^{-1}):

$$\eta = \frac{\sigma}{\dot{\gamma}} \qquad \text{Eq. S8}$$

with σ, the stress (Pa).

Above C_e, HA solutions exhibited a shear-thinning behavior with a plateau at low shear rates. Rheograms were fitted according to the Williamson equation (Eq. S9) [54] using TRIOS software (TA instruments – Waters LCC, New Castle, USA) to determine the zero-shear rate viscosity η_0.

$$\eta = \frac{\eta_0}{1+\left(k\dot{\gamma}\right)^n} \qquad \text{Eq. S9}$$

with *k* (s) the consistency and *n* the power law index.

The specific viscosity η_{sp} was calculated as follows:

$$\eta_{sp} = \frac{\eta - \eta_{solv}}{\eta_{solv}} \text{ or } \eta_{sp} = \frac{\eta_0 - \eta_{solv}}{\eta_{solv}} \qquad \text{Eq. S10}$$

with η_{solv} the viscosity of the solvent at 37°C (HEPES/NaCl 10/115 mM in D_2O, pH 7.4, η_{solv} = 0.89 mPa.s).

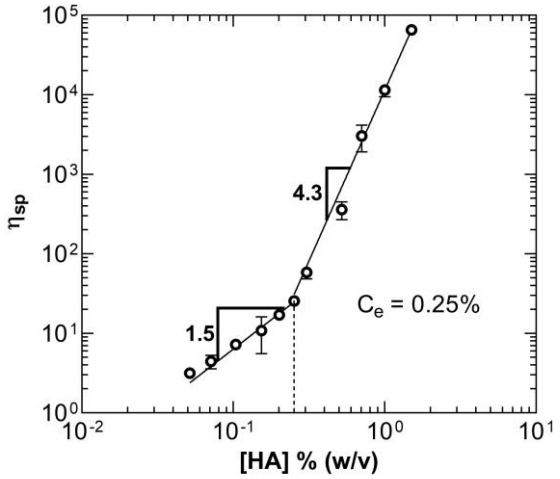

Fig. S5. Determination of the entanglement concentration (C_e) of HA for M_w = 1.14 MDa. Variations of specific viscosity (η_{sp}) as a function of HA concentration. T = 37°C, D_2O buffer (HEPES/NaCl 10/115 mM, pH 7.4). 1.5 and 4.3 are the scaling exponents in semi-dilute unentangled and entangled regimes, respectively.

HA characterization by SANS

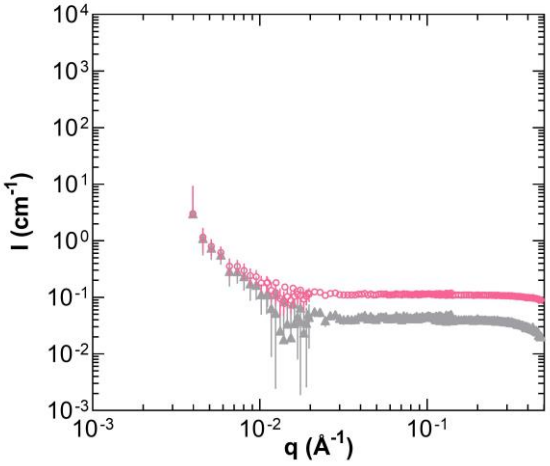

Fig. S6. Scattering intensity curves from D_2O buffer (HEPES/NaCl 10/115 mM, pH 7.4) (▲) and HA at 1.5% w/v (○) in D_2O buffer. T = 37°C.

References

[1] D.J.A. Crommelin, P. van Hoogevest, G. Storm, The role of liposomes in clinical nanomedicine development. What now? Now what?, J. Control. Release. 318 (2020) 256–263. https://doi.org/10.1016/j.jconrel.2019.12.023.

[2] C. Jaudoin, F. Agnely, Y. Nguyen, E. Ferrary, A. Bochot, Nanocarriers for drug delivery to the inner ear: Physicochemical key parameters, biodistribution, safety and efficacy, Int. J. Pharm. 592 (2021) 120038. https://doi.org/10.1016/j.ijpharm.2020.120038.

[3] K. Elkhoury, P. Koçak, A. Kang, E. Arab-Tehrany, J.E. Ward, S.R. Shin, Engineering smart targeting nanovesicles and their combination with hydrogels for controlled drug delivery, Pharmaceutics. 12 (2020) 1–24. https://doi.org/10.3390/pharmaceutics12090849.

[4] M.A. Selyanin, P.Y. Boykov, V.N. Khabarov, F. Polyak, Molecular and Supramolecular Structure of Hyaluronic Acid, in: Hyaluronic Acid, 2015: pp. 97–119. https://doi.org/10.1002/9781118695920.ch4.

[5] M.A. Selyanin, P.Y. Boykov, V.N. Khabarov, F. Polyak, Medical Applications of Hyaluronan, in: Hyaluronic Acid, 2015: pp. 143–192. https://doi.org/10.1002/9781118695920.ch6.

[6] N. El Kechai, E. Mamelle, Y. Nguyen, N. Huang, V. Nicolas, P. Chaminade, S. Yen-Nicolaÿ, C. Gueutin, B. Granger, E. Ferrary, F. Agnely, A. Bochot, Hyaluronic acid liposomal gel sustains delivery of a corticoid to the inner ear, J. Control. Release. 226 (2016) 248–257. https://doi.org/10.1016/j.jconrel.2016.02.013.

[7] L. Lajavardi, S. Camelo, F. Agnely, W. Luo, B. Goldenberg, M.-C. Naud, F. Behar-Cohen, Y. de Kozak, A. Bochot, New formulation of vasoactive intestinal peptide using liposomes in hyaluronic acid gel for uveitis, J. Control. Release. 139 (2009) 22–30. https://doi.org/10.1016/j.jconrel.2009.05.033.

[8] I. Grillo, I. Morfin, J. Combet, Chain conformation: A key parameter driving clustering or dispersion in polyelectrolyte – Colloid systems, J. Colloid Interface Sci. 561 (2020) 426–438. https://doi.org/10.1016/j.jcis.2019.11.010.

[9] S. Asakura, F. Oosawa, On interaction between two bodies immersed in a solution of macromolecules, J. Chem. Phys. 22 (1954) 1255–1256. https://doi.org/10.1063/1.1740347.

[10] S. Asakura, F. Oosawa, Interaction between particles suspended in solutions of macromolecules, J. Polym. Sci. 33 (1958) 183–192. https://doi.org/10.1002/pol.1958.1203312618.

[11] P.G. Bolhuis, E.J. Meijer, A.A. Louis, Colloid-Polymer Mixtures in the Protein Limit, Phys. Rev. Lett. 90 (2003) 068304. https://doi.org/10.1103/PhysRevLett.90.068304.

[12] A. V. Vrij, Polymers At Interfaces And The Interactions in Colloidal Dispersions, Pure Appl. Chem. 48 (1976) 471–483. https://doi.org/10.1351/pac197648040471.

[13] T. Odijk, Depletion theory and the precipitation of protein by polymer, J. Phys. Chem. B. 113 (2009) 3941–3946. https://doi.org/10.1021/jp806722j.

[14] P.-G. De Gennes, Scaling Concepts in Polymer Physics, Cornell University Press, Ithaca, NY, 1979.

[15] R.P. Sear, Entropy-driven phase separation in mixtures of small colloidal particles and semidilute polymers, Phys. Rev. E - Stat. Physics, Plasmas, Fluids, Relat. Interdiscip. Top. 56 (1997) 4463–4466. https://doi.org/10.1103/PhysRevE.56.4463.

[16] R.P. Sear, Scattering from small colloidal particles in a semidilute polymer solution, Eur. Phys. J. B. 1 (1998) 313–317. https://doi.org/10.1007/s100510050188.

[17] R.P. Sear, Phase separation in mixtures of colloids and long ideal polymer coils, Phys. Rev. Lett. 86 (2001) 4696–4699. https://doi.org/10.1103/PhysRevLett.86.4696.

[18] C. Jaudoin, F. Carré, M. Gehrke, A. Sogaldi, V. Steinmetz, N. Hue, C. Cailleau, G. Tourrel, Y. Nguyen, E. Ferrary, F. Agnely, A. Bochot, Transtympanic injection of a liposomal gel loaded with N-acetyl-L-cysteine: A relevant strategy to prevent damage induced by cochlear implantation in guinea pigs?, Int. J. Pharm. 604 (2021) 120757. https://doi.org/10.1016/j.ijpharm.2021.120757.

[19] R. Rowe, P. Sheskey, M. Quinn, Handbook of Pharmaceutical Excipients, Handb. Pharm. Excipients, Sixth Ed. (2009) 549–553. https://doi.org/10.1016/S0168-3659(01)00243-7.

[20] W.H. Haynes, CRC Handbook of Chemistry and Physics, 96th ed., 2016. http://www.hbcpnetbase.com/.

[21] A. Sze, D. Erickson, L. Ren, D. Li, Zeta-potential measurement using the Smoluchowski equation and the slope of the current-time relationship in electroosmotic flow, J. Colloid Interface Sci. 261 (2003) 402–410. https://doi.org/10.1016/S0021-9797(03)00142-5.

[22] A.K. Kenworthy, K. Hristova, D. Needham, T.J. McIntosh, Range and magnitude of the steric pressure between bilayers containing phospholipids with covalently attached poly(ethylene glycol), Biophys. J. 68 (1995) 1921–1936. https://doi.org/10.1016/S0006-3495(95)80369-3.

[23] A. Shah, A.M. Khan, M. Usman, R. Qureshi, M. Siddiq, S.S. Shah, Thermodynamic characterization of dexamethasone sodium phosphate and its complex with DNA as studied by conductometric and spectroscopic techniques, J. Chil. Chem. Soc. 54 (2009) 134–137. https://doi.org/10.4067/S0717-97072009000200007.

[24] J. Santhanalakshmi, G. Shantha Lakshmi, V.K. Aswal, P.S. Goyal, Small-angle neutron scattering study of sodium cholate and sodium deoxycholate interacting micelles in aqueous medium, Proc. Indian Acad. Sci. Chem. Sci. 113 (2001) 55–62. https://doi.org/10.1007/BF02708552.

[25] W.E. Krause, E.G. Bellomo, R.H. Colby, Rheology of Sodium Hyaluronate under Physiological Conditions, Biomacromolecules. 2 (2001) 65–69. https://doi.org/10.1021/bm0055798.

[26] E. Di Cola, I. Grillo, S. Ristori, Small Angle X-ray and Neutron Scattering: Powerful Tools for Studying the Structure of Drug-Loaded Liposomes, Pharmaceutics. 8 (2016) 10. https://doi.org/10.3390/pharmaceutics8020010.

[27] Z. Varga, B. Fehér, D. Kitka, A. Wacha, A. Bóta, S. Berényi, V. Pipich, J.-L. Fraikin, Size Measurement of Extracellular Vesicles and Synthetic Liposomes: The Impact of the Hydration Shell and the Protein Corona, Colloids Surfaces B Biointerfaces. 192 (2020) 111053. https://doi.org/10.1016/j.colsurfb.2020.111053.

[28] S.C. De Smedt, A. Lauwers, J. Demeester, Y. Engelborghs, G. De Mey, M. Du, Structural information on hyaluronic acid solutions as studied by probe diffusion experiments, Macromolecules. 27 (1994) 141–146. https://doi.org/10.1021/ma00079a021.

[29] A. Masuda, K. Ushida, H. Koshino, K. Yamashita, T. Kluge, Novel distance dependence of diffusion constants in hyaluronan aqueous solution resulting from its characteristic Nano-Microstructure, J. Am. Chem. Soc. 123 (2001) 11468–11471. https://doi.org/10.1021/ja016401b.

[30] K.J. Mutch, J.S. Van Duijneveldt, J. Eastoe, I. Grillo, R.K. Heenan, Testing the scaling behavior of microemulsion - Polymer mixtures, Langmuir. 25 (2009) 3944–3952. https://doi.org/10.1021/la802488f.

[31] N. El Kechai, A. Bochot, N. Huang, Y. Nguyen, E. Ferrary, F. Agnely, Effect of liposomes on rheological and syringeability properties of hyaluronic acid hydrogels intended for local injection of drugs, Int. J. Pharm. 487 (2015) 187–196. https://doi.org/10.1016/j.ijpharm.2015.04.019.

[32] S. Peers, P. Alcouffe, A. Montembault, C. Ladavière, Embedment of liposomes into chitosan physical hydrogel for the delayed release of antibiotics or anaesthetics, and its first ESEM characterization, Carbohydr. Polym. 229 (2020) 115532. https://doi.org/10.1016/j.carbpol.2019.115532.

[33] S. Madan, C. Nehate, T.K. Barman, A.S. Rathore, V. Koul, Design, preparation, and evaluation of liposomal gel formulations for treatment of acne: in vitro and in vivo studies, Drug Dev. Ind. Pharm. 45 (2019) 395–404. https://doi.org/10.1080/03639045.2018.1546310.

[34] F. Tuğcu-Demiröz, Vaginal delivery of benzydamine hydrochloride through liposomes dispersed in mucoadhesive gels, Chem. Pharm. Bull. 65 (2017) 660–667. https://doi.org/10.1248/cpb.c17-00133.

[35] S. Kumar, D. Ray, V.K. Aswal, J. Kohlbrecher, Structure and interaction in the polymer-dependent reentrant phase behavior of a charged nanoparticle solution, Phys. Rev. E - Stat. Nonlinear, Soft Matter Phys. 90 (2014) 042316. https://doi.org/10.1103/PhysRevE.90.042316.

[36] S. Kumar, V.K. Aswal, J. Kohlbrecher, Small-Angle Neutron Scattering Study of Interplay of Attractive and Repulsive Interactions in Nanoparticle-Polymer System, Langmuir. 32 (2016) 1450–1459. https://doi.org/10.1021/acs.langmuir.5b03998.

[37] M.Y. Lin, H.M. Lindsay, D.A. Weitz, R. Klein, R.C. Ball, P. Meakin, Universal diffusion-limited colloid aggregation, J. Phys. Condens. Matter. 2 (1990) 3093–3113. https://doi.org/10.1088/0953-8984/2/13/019.

[38] L. Shi, F. Carn, F. Boué, E. Buhler, Role of the ratio of biopolyelectrolyte persistence length to nanoparticle size in the structural tuning of electrostatic complexes, Phys.

Rev. E. 94 (2016) 032504. https://doi.org/10.1103/PhysRevE.94.032504.

[39] J.B. Hooper, K.S. Schweizer, Contact aggregation, bridging, and steric stabilization in dense polymer-particle mixtures, Macromolecules. 38 (2005) 8858–8869. https://doi.org/10.1021/ma051318k.

[40] N. El Kechai, S. Geiger, A. Fallacara, I. Cañero Infante, V. Nicolas, E. Ferrary, N. Huang, A. Bochot, F. Agnely, Mixtures of hyaluronic acid and liposomes for drug delivery: Phase behavior, microstructure and mobility of liposomes, Int. J. Pharm. 523 (2017) 246–259. https://doi.org/10.1016/j.ijpharm.2017.03.029.

[41] X. Ye, T. Narayanan, P. Tong, J.S. Huang, M.Y. Lin, B.L. Carvalho, L.J. Fetters, Depletion interactions in colloid-polymer mixtures, Phys. Rev. E - Stat. Physics, Plasmas, Fluids, Relat. Interdiscip. Top. 54 (1996) 6500–6510. https://doi.org/10.1103/PhysRevE.54.6500.

[42] S. Kumar, M.J. Lee, V.K. Aswal, S.M. Choi, Block-copolymer-induced long-range depletion interaction and clustering of silica nanoparticles in aqueous solution, Phys. Rev. E - Stat. Nonlinear, Soft Matter Phys. 87 (2013) 042315. https://doi.org/10.1103/PhysRevE.87.042315.

[43] J.B. Hooper, K.S. Schweizer, Real space structure and scattering patterns of model polymer nanocomposites, Macromolecules. 40 (2007) 6998–7008. https://doi.org/10.1021/ma071147e.

[44] F. Bordi, S. Sennato, D. Truzzolillo, Polyelectrolyte-induced aggregation of liposomes: a new cluster phase with interesting applications, J. Phys. Condens. Matter. 21 (2009) 203102. https://doi.org/10.1088/0953-8984/21/20/203102.

[45] S. Sennato, L. Carlini, D. Truzzolillo, F. Bordi, Salt-induced reentrant stability of polyion-decorated particles with tunable surface charge density, Colloids Surfaces B Biointerfaces. 137 (2016) 109–120. https://doi.org/10.1016/j.colsurfb.2015.06.011.

[46] M. Ruano, A. Mateos-Maroto, F. Ortega, H. Ritacco, J.E.F. Rubio, E. Guzmán, R.G. Rubio, Fabrication of Robust Capsules by Sequential Assembly of Polyelectrolytes onto Charged Liposomes, Langmuir. 37 (2021) 6189–6200. https://doi.org/10.1021/acs.langmuir.1c00341.

[47] J.E. Scott, Secondary Structures in Hyaluronan Solutions: Chemical and Biological Implications, in: D. Evered, J. Whelan (Eds.), Ciba Found. Symp. 143 - Biol. Hyaluronan, John Wiley & Sons, Ltd, 2007: pp. 6–20. https://doi.org/10.1002/9780470513774.ch2.

[48] A.A.M. Gasperini, X.E. Puentes-Martinez, T.A. Balbino, T. De Paula Rigoletto, G. De Sá Cavalcanti Corrêa, A. Cassago, R.V. Portugal, L.G. De La Torre, L.P. Cavalcanti, Association between cationic liposomes and low molecular weight hyaluronic acid, Langmuir. 31 (2015) 3308–3317. https://doi.org/10.1021/la5045865.

[49] N.N. Sanders, L. Peeters, I. Lentacker, J. Demeester, S.C. De Smedt, Wanted and unwanted properties of surface PEGylated nucleic acid nanoparticles in ocular gene transfer, J. Control. Release. 122 (2007) 226–235. https://doi.org/10.1016/j.jconrel.2007.05.004.

[50] T.D. Edwards, M.A. Bevan, Depletion-mediated potentials and phase behavior for

micelles, macromolecules, nanoparticles, and hydrogel particles, Langmuir. 28 (2012) 13816–13823. https://doi.org/10.1021/la302805n.

[51] A. Guinier, G. Fournet, Small Angle Scattering of X-Rays, Wiley, New York, 1955.

[52] F. Nallet, R. Laversanne, D. Roux, Modelling X-ray or neutron scattering spectra of lyotropic lamellar phases: interplay between form and structure factors, J. Phys. II. 3 (1993) 487–502. https://doi.org/10.1051/jp2:1993146.

[53] J.B. Hayter, J. Penfold, An analytic structure factor for macroion solutions, Mol. Phys. 42 (1981) 109–118. https://doi.org/10.1080/00268978100100091.

[54] M. Milas, M. Rinaudo, I. Roure, S. Al-Assaf, G.O. Phillips, P.A. Williams, Rheological behaviour of hyaluronan, healon and hylan in aqueous solutions, in: J.F. Kennedy, G.O. Phillips, P.A. Williams (Eds.), Hyaluronan, Elsevier, 2002: pp. 181–193. https://doi.org/10.1533/9781845693121.181.